Three-dimensional cooling of a single atom by a pair of counter-propagating tightly focused beams

Gang Li,* Pengfei Zhang, and Tiancai Zhang

State Key Laboratory of Quantum Optics and Quantum Optics Devices, and Institute of Opto-Electronics, Shanxi University, Taiyuan 030006, Shanxi Province, China
*gangli@sxu.edu.cn

Abstract: A light beam tightly focused by a high numerical-aperture lens system contains longitudinal components with polarization parallel to the propagation axis. By numerically analyzing the polarization distribution around the focal region in one pair of confocally aligned counter-propagating tightly focused light beams with orthogonal linear polarizations, we found that there exists a three-dimensional polarization gradient pattern similar to that used in cooling neutral atoms. This can be used to three-dimensionally cool atoms trapped in a far-off-resonant trap with only one pair of counter-propagating beams in one dimension. This new cooling scheme can be used to individually cool single atoms in an addressable two-dimensional single-atom array for quantum information processing and be applied to perform readouts of qubit encoded in these atoms without losing them.

OCIS codes: (020.3320) Laser cooling; (180.0180) Microscopy.

References and links

1. A. Ashkin, "Acceleration and trapping of particles by radiation pressure," Phys. Rev. Lett. **24**(4), 156–159 (1970).
2. J. R. Moffitt, Y. R. Chemla, S. B. Smith, and C. Bustamante, "Recent advances in optical tweezers," Annu. Rev. Biochem. **77**(1), 205–228 (2008).
3. A. M. Kaufman, B. J. Lester, and C. A. Regal, "Cooling a single atom in an optical tweezer to its quantum ground state," Phys. Rev. X **2**(4), 041014 (2012).
4. J. D. Thompson, T. G. Tiecke, A. S. Zibrov, V. Vuletić, and M. D. Lukin, "Coherence and Raman sideband cooling of a single atom in an optical tweezer," Phys. Rev. Lett. **110**(13), 133001 (2013).
5. Z.-H. Wang, G. Li, Y.-L. Tian, and T.-C. Zhang, "Quantum state manipulation of single-Cesium-atom qubit in a micro-optical trap," Front. Phys. **9**(5), 634–639 (2014).
6. A. M. Kaufman, B. J. Lester, C. M. Reynolds, M. L. Wall, M. Foss-Feig, K. R. A. Hazzard, A. M. Rey, and C. A. Regal, "Two-particle quantum interference in tunnel-coupled optical tweezers," Science **345**(6194), 306–309 (2014).
7. T. Li, S. Kheifets, D. Medellin, and M. G. Raizen, "Measurement of the instantaneous velocity of a Brownian particle," Science **328**(5986), 1673–1675 (2010).
8. J. Gieseler, B. Deutsch, R. Quidant, and L. Novotny, "Subkelvin parametric feedback cooling of a laser-trapped nanoparticle," Phys. Rev. Lett. **109**(10), 103603 (2012).
9. L. P. Neukirch, J. Gieseler, R. Quidant, L. Novotny, and A. Nick Vamivakas, "Observation of nitrogen vacancy photoluminescence from an optically levitated nanodiamond," Opt. Lett. **38**(16), 2976–2979 (2013).
10. Y. Minowa, R. Kawai, and M. Ashida, "Optical levitation of a microdroplet containing a single quantum dot," Opt. Lett. **40**(6), 906–909 (2015).
11. R. Huang, I. Chavez, K. Taute, B. Lukic, S. Jeney, M. G. Raizen, and E.-L. Florin, "Direct observation of the full transition from ballistic to diffusive Brownian motion in a liquid," Nat. Phys. **7**(7), 576–580 (2011).
12. T. Li, S. Kheifets, and M. G. Raizen, "Millikelvin cooling of an optically trapped microsphere in vacuum," Nat. Phys. **7**(7), 527–530 (2011).
13. J. Gieseler, R. Quidant, C. Dellago, and L. Novotny, "Dynamic relaxation of a levitated nanoparticle from a non-equilibrium steady state," Nat. Nanotechnol. **9**(5), 358–364 (2014).
14. J. Gieseler, M. Spasenović, L. Novotny, and R. Quidant, "Nonlinear mode coupling and synchronization of a vacuum-trapped nanoparticle," Phys. Rev. Lett. **112**(10), 103603 (2014).
15. J. Gieseler, L. Novotny, and R. Quidant, "Thermal nonlinearities in a nanomechanical oscillator," Nat. Phys. **9**(12), 806–810 (2013).

#237215 Received 31 Mar 2015; revised 20 Jul 2015; accepted 23 Jul 2015; published 31 Aug 2015

16. S. Kheifets, A. Simha, K. Melin, T. Li, and M. G. Raizen, "Observation of brownian motion in liquids at short times: instantaneous velocity and memory loss," Science **343**(6178), 1493–1496 (2014).
17. M. Neugebauer, T. Bauer, A. Aiello, and P. Banzer, "Measuring the transverse spin density of light," Phys. Rev. Lett. **114**(6), 063901 (2015).
18. R. Dorn, S. Quabis, and G. Leuchs, "Sharper focus for a radially polarized light beam," Phys. Rev. Lett. **91**(23), 233901 (2003).
19. J. Dalibard and C. Cohen-Tannoudji, "Laser cooling below the Doppler limit by polarization gradients: simple theoretical models," J. Opt. Soc. Am. B **6**(11), 2023–2045 (1989).
20. M. J. Piotrowicz, M. Lichtman, K. Maller, G. Li, S. Zhang, L. Isenhower, and M. Saffman, "A two-dimensional lattice of blue detuned atom traps using a projected Gaussian beam array," Phys. Rev. A **88**(1), 013420 (2013).
21. T. Xia, M. Lichtman, K. Maller, A. W. Carr, M. J. Piotrowicz, L. Isenhower, and M. Saffman, "Randomized benchmarking of single-qubit gates in a 2D array of neutral-atom qubits," Phys. Rev. Lett. **114**(10), 100503 (2015).
22. X. He, P. Xu, J. Wang, and M. Zhan, "High efficient loading of two atoms into a microscopic optical trap by dynamically reshaping the trap with a spatial light modulator," Opt. Express **18**(13), 13586–13592 (2010).
23. M. Schlosser, S. Tichelmann, J. Kruse, and G. Birkl, "Scalable architecture for quantum information processing with atoms in optical micro-structures," Quantum Inform. Process. **10**(6), 907–924 (2011).
24. M. J. Gibbons, C. D. Hamley, C. Y. Shih, and M. S. Chapman, "Nondestructive fluorescent state detection of single neutral atom qubits," Phys. Rev. Lett. **106**(13), 133002 (2011).
25. A. Fuhrmanek, R. Bourgain, Y. R. P. Sortais, and A. Browaeys, "Free-space lossless state detection of a single trapped atom," Phys. Rev. Lett. **106**(13), 133003 (2011).
26. B. Richards, "Diffraction in systems of high relative aperture," in Astronomical Optics and Related Subjects, Z. Kopal, ed. (North Holland Publishing Company, 1955), pp. 352–359.
27. E. Wolf, "Electromagnetic diffraction in optical systems I. An integral representation of the image field," Proc. R. Soc. Lond. A Math. Phys. Sci. **253**(1274), 349–357 (1959).
28. B. Richards and E. Wolf, "Electromagnetic diffraction in optical systems II. Structure of the image field in an aplanatic system," Proc. R. Soc. Lond. A Math. Phys. Sci. **253**(1274), 358–379 (1959).
29. G. Li, S. Zhang, L. Isenhower, K. Maller, and M. Saffman, "Crossed vortex bottle beam trap for single-atom qubits," Opt. Lett. **37**(5), 851–853 (2012).
30. C. Tuchendler, A. M. Lance, A. Browaeys, Y. R. P. Sortais, and P. Grangier, "Energy distribution and cooling of a single atom in an optical tweezer," Phys. Rev. A **78**(3), 033425 (2008).

1. Introduction

Optical tweezers formed by tightly focusing a laser beam through an optical system of high numerical aperture (NA) could produce three-dimensional (3D) gradient forces and hold small particles around the focus. Following its first introduction by Ashkin in 1970 [1], it has been widely applied in trapping various particles, such as dielectric spheres and bio-particles, with size varying from sub-nanometer to micrometers to study various (bio- or physics) processes in many fields [2]. In the field of quantum physics, it can be used to trap single neutral atoms [3–5] and to study their basic quantum behaviors [6]. More recently, it has been used to trap dielectric micro- or nano-particles [7–10] to investigate the thermodynamic processes [11–16] and macro-quantum phenomena.

Because of the refraction of the lens, a tightly focused beam contains a longitudinal field component around the focal region which has been directly measured by the scattering of dipole-like plasmonic gold nanoparticles [17]. These longitudinal components could change the trap size and structure. In a trap established by a linear polarization beam, the longitudinal components make the trap size in the polarization direction smaller. Moreover, using a radially polarized light beam, one can get a radially symmetric focal spot with much smaller size than that from linearly polarized light [18]. Usually, such modifications of the trap size make the manipulation of the trapped particle more convenient. For a trapped neutral atom or a dielectric particle in an optical tweezers, a smaller trap size corresponds to a higher trapping frequency and the resulting difference in the radial trap sizes decouples the particle motion in the radial directions. This provides an additional mutually-independent particle motion in all three directions. Using various cooling methods, dielectric micro- (or nano-) particles can be cooled to several milli-Kelvin [7,8] and single neutral atoms can be cooled to their vibrational ground states [3,4]. However, in neutral-atom manipulation experiments, the longitudinal components degrade the coherence of the atomic internal state and make it difficult to control [4].

In conventional neutral-atom trapping experiments, the tightly focused beams are only used for trapping. In our study, we have analyzed the field polarization distribution composed

#237215 Received 31 Mar 2015; revised 20 Jul 2015; accepted 23 Jul 2015; published 31 Aug 2015

of longitudinal and transversal field components around the foci region in only one pair of confocally aligned counter-propagating tightly focused light beams with orthogonal linear polarizations. We obtained 3D polarization gradient patterns similar to those present in polarization gradient cooling (PGC) of neutral atoms [19]. Using proper field frequency detuning, it is expected to cool neutral atoms in all three dimensions. This proposal greatly simplifies the atomic cooling configuration and can be used to cool individual atoms in an addressable 2D neutral atom array [20–23]. One can also use it to perform readouts of a qubit encoded in a single atom without it being lost [24, 25].

2. Polarization distributions in counter-propagating tightly focused beams

Figure 1 depicts the configuration in which a collimated beam with linear polarization along the x axis is tightly focused by an ideal high NA lens system. After refraction by the lens system, light rays on the Gaussian reference sphere have the same phase and the corresponding electric field strength is determined by the input beam mode. All the beam rays converge to the focal point and the electric field distribution at any point *P(x,y,z)* around the focus is described by the well-known Debye-Wolf integral [26–28]

$$E(x,y,z) = -\frac{ik}{2\pi}\iint_{\Omega}\frac{a(s_x,s_y)}{s_z}\exp[ik(s_x x + s_y y + s_z z)]ds_x ds_y, \qquad (1)$$

where $k = 2\pi n/\lambda$ is the wave number with media refraction index n and wavelength λ, $a(s_x,s_y)$ the electric strength vector at the Gaussian reference sphere [27], $\vec{s} \equiv (s_x,s_y,s_z)$ the unit vector along the light ray, and Ω is the solid angle covered by the exit pupil of the lens system.

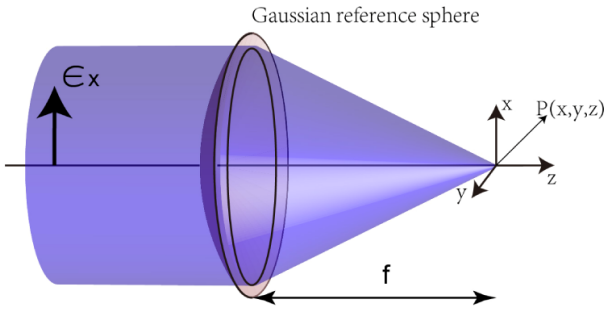

Fig. 1. Geometry of the Debye–Wolf integral

Given all the parameters in a realistic lens system, we can calculate the amplitude and phase distributions of the electric field around the focus using Eq. (1). To characterize the distributions for different electric components, we adopt the following parameter settings for our calculation: a lens system with NA = 0.55 and focal length f = 18 mm, and an input Gaussian beam with waist w_0 = 10 mm, wavelength λ = 852 nm, and polarization along the x direction. The corresponding electric field distributions, specifically E_x (the component along the x direction) and E_z (component along the z direction) on the x-z plane (y = 0) are displayed in Fig. 2. The electric field E_y (component with polarization along the y direction) is not considered here because it is usually at least one order of magnitude smaller than the other two. Their features are: 1) the amplitude of E_x has one maximum at the focal point and smoothly spreads out in all directions, whereas amplitude of E_z has two maxima that reside on both sides of the z axis and is 0 on the z axis (With higher NA, there is a relatively stronger E_z; 2) E_x has a symmetric phase distribution along the z axis and the phase of E_z undergoes a p change at z = 0 in x direction.

Consider now a pair of confocally aligned counter-propagating tightly focused light beams B_1 and B_2 with orthogonal linear polarizations along the x and y directions, respectively (Fig.

#237215 Received 31 Mar 2015; revised 20 Jul 2015; accepted 23 Jul 2015; published 31 Aug 2015

3). In the focal region, the electric components E_{1x} from beam B_1 with polarization along the x axis and E_{2y} from beam B_2 with polarization along the y axis form a polarization distribution along the z direction. The polarization is analogous to the PGC scheme with an "lin ⊥ lin" configuration [19], which can be used to cool atoms moving on the z direction. Moreover, the E_{1x} (E_{2y}) from beam B_1 (B_2) with polarization along the x (y) axis and E_{2z} (E_{1y}) from beam B_2 (B_1) with polarization along the z axis forms a polarization gradient along the y (x) axis, which also can be used to dissipate kinetic energy from an atom moving radially.

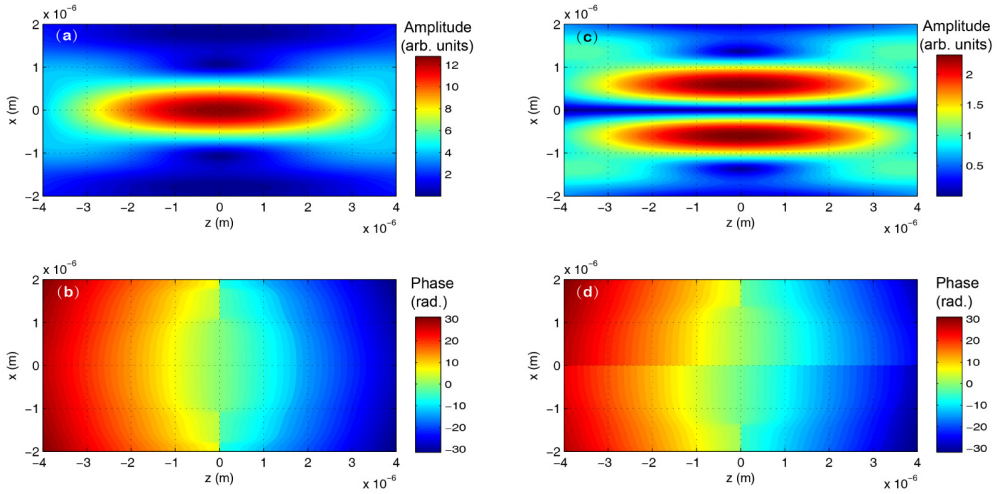

Fig. 2. Amplitude and phase distributions for the transverse electric field components (E_x components, (a) and (b)) and longitudinal electric field components (E_z components, (c) and (d)) on the z-x plane around the focal point in a tightly focused beam with linear polarization. The figures are calculated based on parameter settings NA = 0.55, focal length f = 18 mm, input beam waist w_0 = 10 mm and wavelength λ = 852 nm. Figures 4 and 5 below are based on the same parameters.

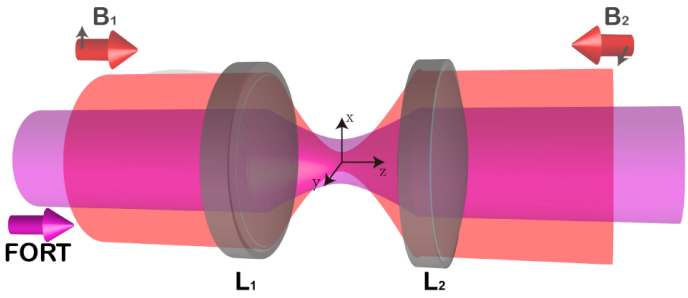

Fig. 3. Scheme of atom cooling by a pair of confocally aligned counter-propagating tightly focused light beams (B_1 and B_2) with orthogonal linear polarizations. The FORT has a bigger trap size and overlaps with the tightly focused beam.

To give a more specific interpretation, we shall analyze the composed polarization distribution along each direction. The degree of circularity (DOC) for a field composed of two orthogonally polarized components at a point can be calculated using

$$q = \frac{2E_1E_2}{E_1^2 + E_2^2}\sin\Phi, \tag{2}$$

where E_1 and E_2 are two field amplitudes with polarizations orthogonal to each other and F the phase lag between them. The DOC gives a measure of the polarization circularity with q =

#237215 Received 31 Mar 2015; revised 20 Jul 2015; accepted 23 Jul 2015; published 31 Aug 2015

−1, 0, and + 1 representing polarizations of σ^-, π, and σ^+, respectively, and other values correspond to elliptically polarized field. When the composed field interacts with the atom, the corresponding light shift for state $|nS_{1/2}, F, m_F\rangle$ can be expressed as

$$U(F, m_F) = \alpha_F E^2 + \beta_F q g_F m_F E^2, \tag{3}$$

where α_F and β_F are the scalar and vector polarizabilities, E the composed field amplitude with $E^2 = E_1^2 + E_2^2$, and g_F the Landé g factor.

Using Eq. (2) and the upper computed E_{1x} and E_{2y}, we obtain the DOC distribution composed by E_{1x} and E_{2y} [Fig. 4(a)]. From this figure, we see that the composed polarization varies repeatedly from right circular to linear and then to left circular along the z direction and this is exactly the PGC setting with an "lin ⊥ lin" configuration. Plots of the ground-state light shift for an atom with simple level structure (inset of Fig. 4(b)) are also displayed in Fig. 4(b). Using the proper cooling beam parameters, atoms moving along the z axis experience successive "Sisyphus" cooling and lose their kinetic energy.

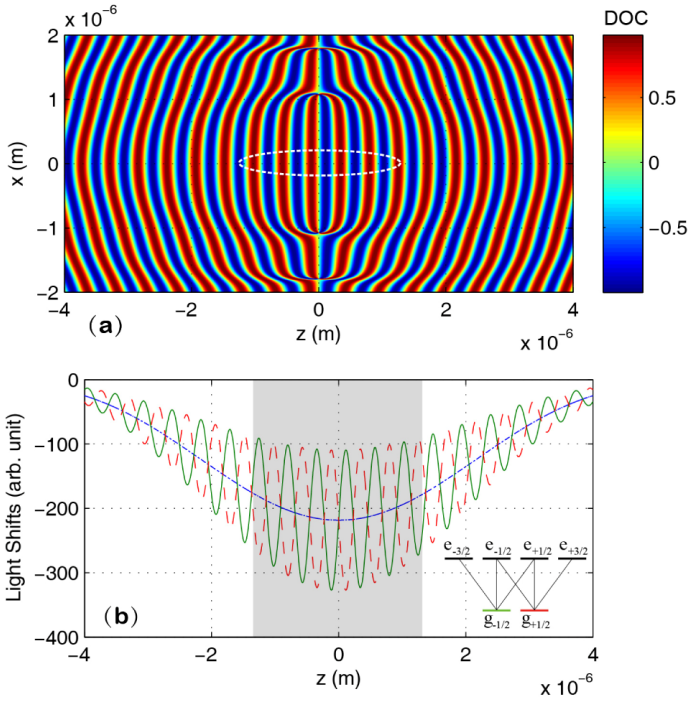

Fig. 4. (a) The DOC distribution composed by E_{1x} and E_{2y} on the z-x plane. (b) The corresponding light shift of the ground state on the z axis when the atom interacts with the tightly focused beams. Here the green solid line and red dashed line are for state $|g_{-1/2}\rangle$ and $|g_{+1/2}\rangle$ and blue dash-dotted line is light shift for linear polarized beam and is for reference here. For simplification we consider atoms with level structure shown in the inset of (b). The region inside the dashed lines in (a) and the shaded area in (b) indicate position variance of a Cesium oscillator with temperature of 100 μK trapped in a size of 2μm FORT by 1064nm laser as descripted in the main text.

The polarization distribution composed by E_{1x} and E_{2z} can also be calculated in the same way. In Fig. 5(a), we give the corresponding DOC distribution on the y-z plane with phase delay of $\pi/2$ at the origin of the coordinate system. We see that there exist polarization distributions along the y direction. At points $z = 0, \pm \lambda/4, \pm \lambda/2, \ldots$, the DOC varies from negative to positive, which means the polarization varies from σ^+ to π and then to σ^-. A typical DOC distribution on the y-x plane at $z = 0$ [Fig. 5(b)] shows that the value of DOC

#237215 Received 31 Mar 2015; revised 20 Jul 2015; accepted 23 Jul 2015; published 31 Aug 2015

varies from −1 to + 1. Hence, the tightly focused beams can provide "Sisyphus" cooling on the y axis at these points. However, at points $z = \pm \lambda/8, \pm \lambda 3/8, \ldots$, the DOC is about 0 along the y axis corresponding to linear polarization. A detailed calculation shows that the corresponding angle between the composed field polarization and the z-y plane is continuously rotating along the y axis at these points. A typical polarization angle distribution

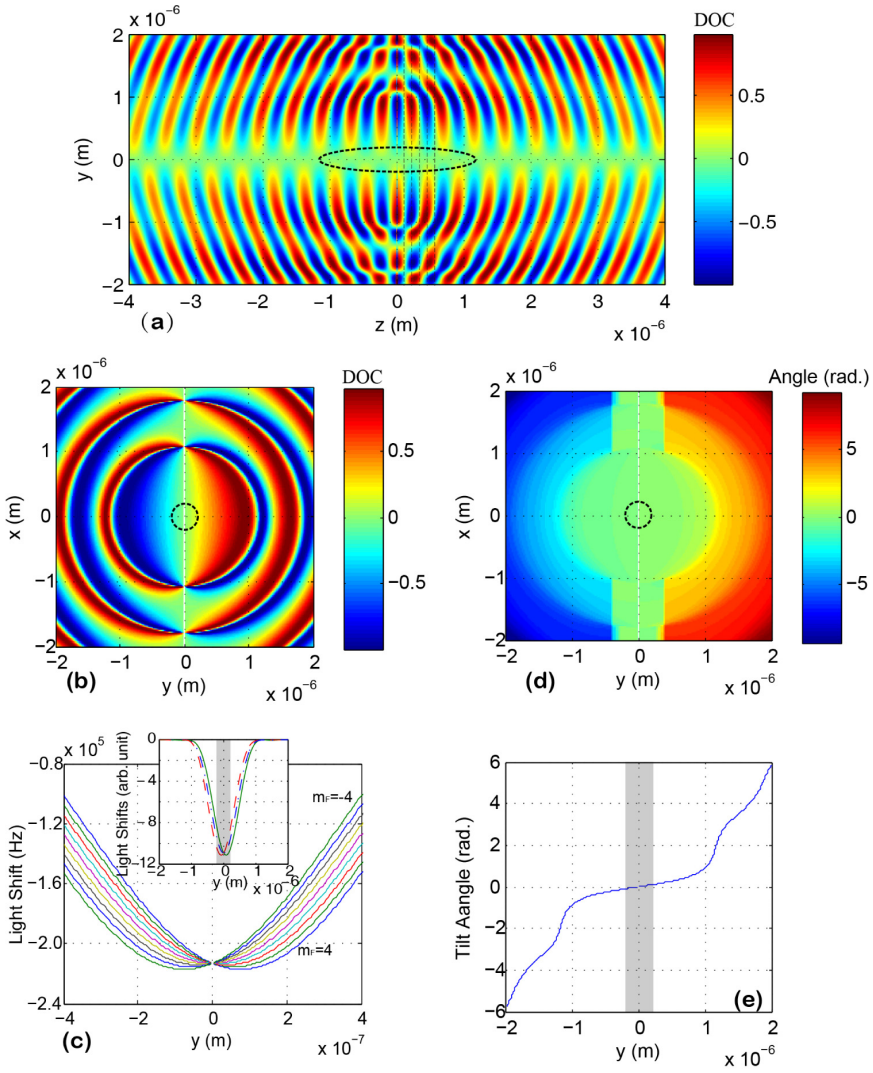

Fig. 5. (a) DOC distribution composed by E_{1x} and E_{2z} on the z–x plane with phase delay of $\pi/2$ at the origin of the coordinate system. The black dashed vertical lines on the right side of $z = 0$ correspond sequentially to $z = \lambda/8, \lambda/4, 3\lambda/8, \lambda/2, 5\lambda/8$. (b) The DOC distribution in y–x plane at z = 0 in (a). (c) The light shift for the Cesium atom ground state F = 4 in the central region of the tightly focused beams; the lines correspond in sequentially to $m_F = -4$ to $m_F = 4$. The inset shows the corresponding light shift in the ground state with simple atomic state structure (inset of Fig. 4(b)) on the y axis when the atom interacts with the tightly focused beams, where the green solid line and red dashed line are for state $|g_{+1/2}\rangle$ and $|g_{-1/2}\rangle$; the blue dash-dotted line is the light shift for a linear polarized beam given as reference. (d) The polarized angle distribution in the y–x plane at $z = \lambda/8$ in (a), where the composed field is linear polarized. (e) The polarized angle distribution along the y at $x = 0$ in (d). The region inside the dashed lines in (a), (b), (d) and the shaded area in (c) and (e) indicate the position variance of a Cesium oscillator with temperature of 100 μK and trap size of 2μm FORT by 1064 nm laser as described in the main text.

#237215 Received 31 Mar 2015; revised 20 Jul 2015; accepted 23 Jul 2015; published 31 Aug 2015

for $z = \lambda /8$ is shown in Fig. 5(c).The polarization gradient is quite similar to the PGC with a "$\sigma^+ - \sigma^-$" configuration and will also provide cooling along the y axis. The polarization gradients along the y axis in other places contain both polarization patterns and therefore both types of cooling occur.

The polarization distribution composed by E_{2y} and E_{1z} on the z–x plane is the same as that composed by E_{1x} and E_{2z} on the z–y plane and will provide a similar cooling mechanism along the x direction. Thus, a pair of confocally aligned counter-propagating tightly focused light beams with orthogonal linear polarizations provides cooling along all three directions, simultaneously. However, because of the very small size of the focused beam, these cooling effects would not effectively work for those atoms out of the focal region. To ensure the mechanism functions, a far-off-resonant trap (FORT) with micrometer size needs to be introduced. The position of the FORT should overlap exactly with the tightly focused beams. The FORT would then trap the atom and confine the atomic motion in a limited space while the overlapped tightly focused beams cool it.

3. Cooling atoms in FORT with counter-propagating tightly focused beams

From Fig. 2, we can see that the working distance of the forenamed cooling mechanism is limited by the small focused beam sizes, which are usually several micrometers and sub-micrometers on axial (z) and radial (x and y) directions. Free atoms would transit through the beam before the corresponding cooling mechanisms work. This problem can be fixed by considering a realistic situation whereby a mm-size FORT overlaps a tightly focused beam. The FORT will load atoms from an atomic ensemble, which is usually cooled and trapped using a magneto-optical trap (MOT). The loaded atom is trapped and moves back and forth in the semi-harmonic trap. The position variance of the trapped atom and the vibration amplitude of the singe-atom harmonic oscillator depend on the trap structure and trap depth, and are usually on the micrometer level. For example, we consider a FORT forming by focusing a 1064 nm laser beam to the size of 2 μm with trap depth of about 1 mK. This trap loads and traps Cesium atoms precooled by MOT with temperature T_a = 100 μK. The corresponding position variances on axial (z) and radial (x and y) directions are about 2.6 μm and 320 nm, respectively, which match the cooling distances of the currently discussed system.

In this kind of FORT, energy dampening is a little different from that in conventional PGC with parallel beams. In conventional PGC with a "lin ⊥ lin" configuration [19], the freely moving atom continuously climbs the potential hill in one direction and loses kinetic energy by pumping back to a lower energy level, and the velocity is hence decreased at the same time. In our case, the atom is trapped in a FORT and it oscillates back and forth in the FORT, where the motion of the trapped atom covers only small part of the polarization gradient and the atom undergoes a transient maximum velocity in the bottom of the FORT and stops instantaneously at the highest potential energy. The friction force that the atom experienced varies between its maxima and minima with frequency same to atomic oscillation. Thus the averaged friction force over atomic oscillation period is much smaller than that of a freely moving atom in conventional PGC process. So, the corresponding kinetic energy damping rate will be much slower.

Here we consider a one-dimensional atom motion along the y direction. At points $z = 0, \pm \lambda /4, \pm \lambda /2, \ldots$ in Fig. 5(a), the polarization is similar to the "lin ⊥ lin" configuration. Under confinement by the FORT, the atom oscillates in the central region of the field where the DOC changes a little. In Fig. 5(b), we show the DOC distribution on the x–y plane (z = 0) and the range of atom motion. For simplicity, we consider an atomic level scheme [inset of Fig. 4(b)]; the corresponding ground state light shift along the y axis is shown in the inset of Fig. 5(c). The atomic oscillator will stop at both sides of the potential hill of the FORT where the composed polarization is partially σ^+ (or partially σ^-). We start from the left-hand side where the atom is optically pumped by the composed partial σ^- field to provide a greater population of the $|g_{-1/2}\rangle$ state. During its transfer to the right-hand side the population will not change if the life time of ground state τ_p is long enough. Once it stops on the right-hand side, the

#237215 Received 31 Mar 2015; revised 20 Jul 2015; accepted 23 Jul 2015; published 31 Aug 2015

partial σ^+ field pumps it to the $|g_{-1/2}>$ state and increases the population of this state. Because the $|g_{-1/2}>$ state has lower energy than the $|g_{+1/2}>$ state, the atom relinquishes some of its kinetic energy. When atoms move back and forth in the FORT, they lose kinetic energy continuously. We can see here that the most efficient damping occurs when $\tau_p = T_r/2$, where T_r is the atomic oscillation period in the radial directions. For a real atom, τ_p is determined by the light frequency detuning ΔD and intensity I by

$$\frac{1}{\tau_p} = \left(\frac{\Gamma}{2}\right)\frac{I/I_{sat}}{1+4(\Delta/\Gamma)^2+(I/I_{sat})}, \tag{4}$$

where I_{sat} is the saturation intensity for the corresponding transition, and Γ the decay rate. Hence, it is easy to optimize the beam to achieve an efficient cooling. For a Cesium atom trapped in the FORT by a 1064-nm laser, if the frequency detuning $\Delta = -7\Gamma$ and the maximum intensity $I = I_{sat}$, we obtain the corresponding light shift of the ground state [Fig. 5(c)] and the lifetime τ_p = 12.1 μs. The trap frequency in the radial direction is $2\pi \times 40$ kHz, and the corresponding oscillation period T = 25 μs. Thus, we can achieve an efficient cooling. At points along $z = \pm \lambda/8, \pm \lambda\ 3/8, \ldots$, the atom experiences a rotating linear polarization, and the unbalanced radiation pressure induced by the motion-induced atomic ground state orientation [19] works around the trap bottom, where the atom moves. In the setup with a Cesium atom, the angle of the rotating polarization that the atom experiences along y at $z = \lambda/8$ is about 9.5 degrees; see Fig. 5(d) and (e). In trap experiments using single Cesium or Rubidium atoms with a micro-size FORT, where the conventional PGC with "σ^+–σ^-" is applied to cool atom [29,30], the atomic oscillator only experiences a rotation angle of order of about ten degrees and the atom can be efficiently cooled. Hence, efficient cooling can also be expected at these points. At other points on the z axis, both cooling mechanisms will work.

Consider the current discussing instance that single Cesium atom is trapped with initial temperature about 100 μK, which means a positon varying range from –160 nm to 160 nm in radial (y). The corresponding DOC changes from –0.16 to + 0.16 at point z = 0 [Fig. 5 (b)] and the corresponding polarization rotation angle is from –4.7 degree to + 4.7 degree at points $z = \pm \lambda/8$ [Figs. 5(d) and 5(e)]. The situation could be simulated by using two counter-propagating collimated beams along y axis with effective wavenumber of $k_{\text{eff}} = 2\pi/12$ μm^{-1} in "lin $\perp$ lin" or "σ^+–σ^-" PGC configurations to cool the atomic oscillator locates around y = 0 with vibration amplitude of about 160 nm. The simulation beams have equal amplitudes E_0 and the total electric field is

$$E(y,t) = E_0\left(\varepsilon e^{ik_{eff}y} + \varepsilon' e^{-ik_{eff}y}\right)\exp(-i\omega t) + c.c., \tag{5}$$

where ε and ε' are the polarizations. ω is the beam frequency. Thus, the cooling efficiency in y direction can be calculated by following the procedures given by Dalibard and Cohen-Tannoudji [19]. For simplicity we only concern $J_g = 1/2 \longleftrightarrow J_e = 3/2$ and $J_g = 1 \longleftrightarrow J_e = 2$ atomic structures and transitions in the simulated "lin $\perp$ lin" and "σ^+–σ^-" PGC configurations.

For the cooling with "lin $\perp$ lin" configuration, we can finally get the expression of the force that the atom experienced with

$$f(y,v) = \frac{2}{3}\hbar k_{eff}\delta s_0 \sin(2k_{eff}y)\frac{\cos(2k_{eff}y) + 2k_{eff}v\tau_p \sin(2k_{eff}y)}{1+4v^2{\tau_p}^2}, \tag{6}$$

where $y = \sqrt{2E/(m\omega^2)}\sin(\omega_0 t + \phi)$ and $v = \sqrt{2E/m}\cos(\omega_0 t + \phi)$ are position and velocity of atomic oscillator, E, m, ω_0 and ϕ stand for the energy, mass, vibration frequency and phase of

#237215 Received 31 Mar 2015; revised 20 Jul 2015; accepted 23 Jul 2015; published 31 Aug 2015

the atomic oscillator, respectively; $\hbar$ and δ are Planck constant and beam frequency detuning; $s_0 = \left(\Omega^2/2\right)/\left(\delta^2 + \Gamma^2/4\right)$ is the detuning-dependent saturation parameter with Ω the Rabi frequency. In the current discussing case, the atom oscillates around $y = 0$ with $k_{eff} y \ll 1$ and $v\tau_p \ll 1$, so Eq. (6) can be simplified to

$$f(y,v) = \frac{2}{3}\hbar k_{eff}\delta s_0 (2k_{eff} y) + \frac{4}{3}\hbar {k_{eff}}^2 \delta s_0 v\tau_p (2k_{eff} y)^2. \quad (7)$$

The first part in right side of Eq. (7) is proportional to the oscillation amplitude which is 0 when averaging over time. The second part is the friction force, which is proportional to the atom velocity *v* and will consume the kinetic energy of atom. Thus, the corresponding friction coefficient is

$$\alpha_1 = -\frac{4}{3}\hbar {k_{eff}}^2 \delta s_0 \tau_p (2k_{eff} y)^2. \quad (8)$$

We can see the friction force is maxima when the atomic oscillator gets to its maximum amplitude. Because the oscillation period is much shorter than the energy dissipation time scale, the friction coefficient should be averaged over the oscillation period and thus can be expressed as

$$\bar{\alpha}_1 = -\frac{16}{3}\hbar {k_{eff}}^4 \delta s_0 \tau_p \frac{E}{m\omega_0^2}. \quad (9)$$

For the cooling with $J_g = 1 \longleftrightarrow J_e = 2$ atomic structure in "$\sigma^+ - \sigma^-$" configuration in our case, by following the procedure in Ref [19]. we can finally get friction coefficient:

$$\alpha_2 = \frac{120}{17}\frac{-\delta\Gamma}{5\Gamma^2 + 4\delta^2}\hbar {k_{eff}}^2, \quad (10)$$

which is formally same to the expression in Ref [19]. and is constant once the frequency detuning is set.

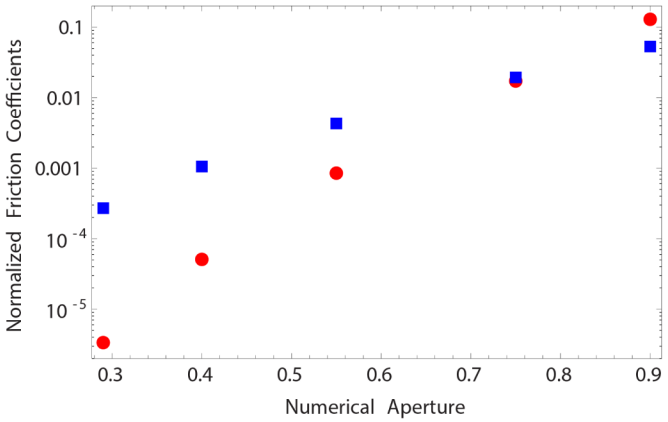

Fig. 6. Normalized friction coefficients produced by lens systems with different NA numbers. The friction coefficients are normalized to the values in conventional PGC of free moving atoms by "lin ⊥ lin" and "$\sigma^+ - \sigma^-$" configurations with same parameters. Blue solid squares and red solid circles are corresponding to "$\sigma^+ - \sigma^-$"and "lin ⊥ lin" configurations, respectively. The NA numbers used for calculation in figure are 0.29, 0.4, 0.55, 0.75 and 0.9. All the data are calculated under the following parameters: lens aperture = 23.6 mm, incident Gaussian beam waist = 10 mm, beam wavelength = 852 nm, trapping frequency $\omega_0 = 2\pi \times 40$ kHz, atom temperature = 100 μK.

#237215 Received 31 Mar 2015; revised 20 Jul 2015; accepted 23 Jul 2015; published 31 Aug 2015

Compare to friction coefficients in the conventional PGC of free moving atoms by "lin ⊥ lin" and "$\sigma^+-\sigma^-$" configurations in Ref [19]. by the laser beams at 852nm with the same detunings and intensities, these friction coefficients are about 1000 and 200 times smaller respectively when the atom temperature is 100 μK in the current discussing NA = 0.55 instance. The coefficients are limited by small effective wavenumber k_{eff}, which could be increased by using more tightly focused beams with higher NA lens systems. Some of the friction coefficients produced by different NA lens systems are calculated and shown in Fig. 6. Here the friction coefficients are normalized to the values in conventional PGC of free moving atoms by "lin ⊥ lin" and "$\sigma^+-\sigma^-$" configurations. We can see that the friction coefficients could be increased dramatically by using lens system with very high NA number. Lower NA lens system provides very small friction coefficients which need a very long time to dissipate the kinetic energy.

With the friction coefficients, the dissipation of kinetic energy E could be calculated by using

$$\frac{dE}{dt} = -\alpha v^2. \tag{11}$$

Figures 7(a) and 7(b) show the energy dissipation processes in current discussing NA = 0.55 instance. The energy dissipation processes with same beam parameters in conventional PGC are also shown for references. We can see the energy of FORT-trapped atom can still be effectively dissipated for longer time scale even with very small friction coefficients.

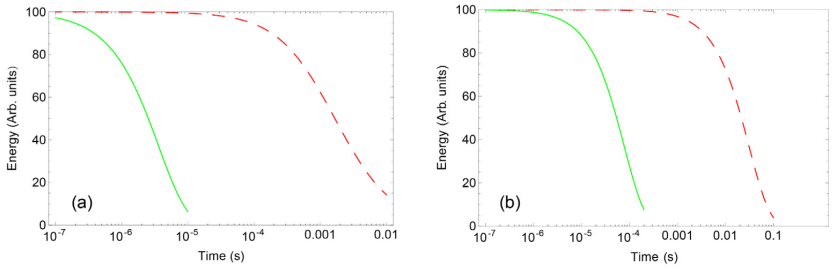

Fig. 7. (a) Energy dissipation with time by "lin ⊥ lin" configuration in current discussing tightly focused instance (red dashed line) and conventional PGC (green solid line). (b) Energy dissipation with time by "$\sigma^+-\sigma^-$" configuration in current discussing tightly focused instance (red dashed line) and conventional PGC (green solid line). All the lines are produced by using following parameters and relations: beam wavelength = 852 nm, detuning $\delta = -7\Gamma$, trapping frequency $\omega_0 = 2\pi \times 40$ kHz and $1/\tau_p = 2\Gamma s_0/9$ as shown in Ref [19].

To maximize the radial cooling efficiency, the atom must be slow enough along the axial (z) direction so that the atom oscillates more times in the same radial cooling configuration [see Fig. 5(a)]. Thus, we need $v_z < \lambda/2T_r$, where v_z is the maximum velocity of the atom on the z axis, λ the cooling beam wavelength, and T_r the oscillation period on radial directions. The lower v_z is, the higher the cooling efficiency is radially. In our setup with a Cesium atom in a 1064-nm FORT, to ensure the cooling mechanism in the radial directions works effectively, the corresponding temperature T_z on the z axis needs to be lower than 79 μK. Fortunately, the temperature along the z axis can be decreased with very high efficiency. In the z direction, because of a relative loose confinement of the FORT, the amplitude of the atomic oscillator overlaps with several potential hills [Fig. 4(b)]. The cooling process is then analogous to a conventional PGC with a "lin ⊥ lin" configuration and the cooling efficiency is much higher than that obtained radially. The radial atom motion can thus be cooled down sufficiently so that the cooling mechanics in the radial direction works efficiently and thereby the counter-propagating tightly focused beams can cool atoms trapped in the FORT in all three dimensions.

#237215 Received 31 Mar 2015; revised 20 Jul 2015; accepted 23 Jul 2015; published 31 Aug 2015

4. Conclusion

In this paper, we have proposed a new cooling scheme that involves simply a counter-propagating strongly focused beam. Numerical calculations and theoretical analysis show that there exists a 3D polarization gradient pattern which can be used to cool neutral atoms trapped in a FORT. Because the tightly focused beam has small size, one needs only pW power for each beam, and sufficient overlap between the FORT and the tightly focused beams. This new cooling scheme can be used to individually cool single atoms in an addressable 2D single-atom array for quantum information processing. Moreover, it can also be used to perform readouts of qubit data encoded in single atoms without losing them.

Acknowledgments

The work was supported by the Major State Basic Research Development Program of China (Grant No. 2012CB921601) and the National Natural Science Foundation of China (Grant No. 61275210, 11125418, 61227902, 91336107, and 61121064).

#237215 Received 31 Mar 2015; revised 20 Jul 2015; accepted 23 Jul 2015; published 31 Aug 2015